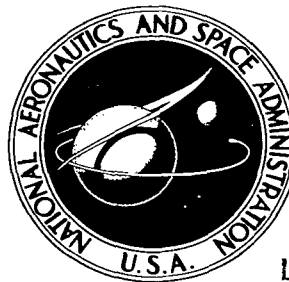


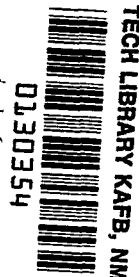
**NASA TECHNICAL NOTE**



**NASA TN D-3499**

*c. 1*

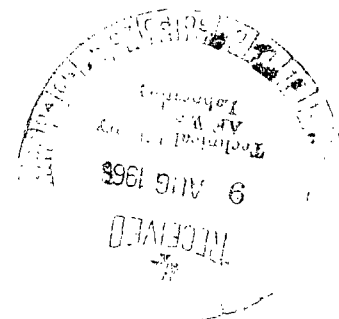
LOAN COPY: RETL  
AFWL (WLIL-  
KIRTLAND AFB, N



**NASA TN D-3499**

# DYNAMIC-MODEL STUDY OF PLANETARY-ENTRY CONFIGURATIONS IN THE LANGLEY SPIN TUNNEL

*by Peter J. Costigan*  
*Langley Research Center*  
*Langley Station, Hampton, Va.*





DYNAMIC-MODEL STUDY OF PLANETARY-ENTRY CONFIGURATIONS  
IN THE LANGLEY SPIN TUNNEL

By Peter J. Costigan

Langley Research Center  
Langley Station, Hampton, Va.

NATIONAL AERONAUTICS AND SPACE ADMINISTRATION

---

For sale by the Clearinghouse for Federal Scientific and Technical Information  
Springfield, Virginia 22151 - Price \$1.00

DYNAMIC-MODEL STUDY OF PLANETARY-ENTRY CONFIGURATIONS  
IN THE LANGLEY SPIN TUNNEL

By Peter J. Costigan  
Langley Research Center

SUMMARY

A study has been conducted in the Langley spin tunnel to determine the low subsonic speed stability and drag characteristics during vertical descent of a number of entry configurations being considered for probes of planetary atmospheres. The models tested were three of a series designated as tension shells, two blunted cones, a configuration similar to the Apollo command module, a sphere, a step-sphere, a hemisphere, and two modified spheres.

The results of the study indicate that the tension shells had a limit-cycle oscillation of less than  $\pm 20^\circ$  and had the highest drag coefficients of any of the configurations tested. These configurations would not return to erect positions if launched inverted, but would tumble after several increasingly large oscillations.

An appendix treats the problem of scaling techniques necessary to simulate planetary environments other than that of the Earth.

INTRODUCTION

The National Aeronautics and Space Administration is presently concentrating much effort on unmanned space probes in an attempt to gather information necessary for post-Apollo space exploration. Included in this effort will be the landing of instrument packages on various planets. The first instrument packages will probably be atmospheric probes designed to collect and transmit data including the density and temperature of planetary atmospheres. These instrument packages will be enclosed in capsules which must be designed to survive entry into a planetary atmosphere and, after deceleration, to descend in a stable attitude to the surface of the planet. For a more complete description of the mission and design considerations for a probe of the Martian atmosphere, see reference 1. In order to aid in the selection of a configuration with satisfactory stability characteristics and sufficiently high drag coefficient to limit the equilibrium rate of descent, a study has been conducted in the Langley spin tunnel on a number of planetary entry capsule configurations being considered for use in this project.

Previous investigations in the Langley spin tunnel have repeatedly demonstrated the feasibility of simulating certain motions of aircraft and spacecraft in the Earth's environment with small-scale dynamic models. (See, for example, refs. 2, 3, and 4.) Extending this procedure to simulate motions of vehicles in planetary environments other than that of the Earth requires methods of correcting for the different gravitational field and the different atmospheric density of the particular planet, so consideration was given to this problem during the investigation.

Based on latest available information, the sea-level pressure of the Martian atmosphere is thought to be between 5 and 10 millibars. The lack of certainty with respect to the atmospheric pressure and the lack of data on the effects of variation of Reynolds number on the configurations tested are such that the present tests must be considered to be of an exploratory nature, and caution must be exercised in the application of the results of these tests to full-scale configurations.

#### SYMBOLS

$A_m$	cross-sectional area of model, $\pi r_{b,m}^2$ , centimeter <sup>2</sup>
$A_p$	cross-sectional area of full-scale configuration, $\pi r_{b,p}^2$ , centimeter <sup>2</sup>
$C_D$	drag coefficient, $\frac{\text{Drag force}}{\frac{1}{2}\rho_e V_m^2 A_m}$
$C_m$	pitching-moment coefficient, $\frac{\text{Pitching moment}}{\frac{1}{2}\rho_e V_m^2 A_m r_{b,m}}$
$f_m$	oscillation frequency of model on Earth, second <sup>-1</sup>
$f_p$	oscillation frequency of full-scale configuration on planet, second <sup>-1</sup>
$g_e$	acceleration due to gravity on Earth, 980 centimeters per second <sup>2</sup>
$g_p$	acceleration due to gravity on planet, centimeters per second <sup>2</sup>
$I_X, I_Y, I_Z$	moments of inertia of model about X-, Y-, and Z-body axes, gram-centimeter <sup>2</sup>
$I_m$	model-scale moment of inertia, $m_m k_m^2$ , gram-centimeter <sup>2</sup>

$I_p$	full-scale moment of inertia, $m_p k_p^2$ , gram-centimeter <sup>2</sup>
$k_m$	model-scale radius of gyration, centimeter
$k_p$	full-scale radius of gyration, centimeter
$m_m$	model-scale mass, grams
$m_p$	full-scale mass, grams
$N$	scale ratio of model to full-scale configuration
$q$	angular velocity, radians per second
$\dot{q}_m$	model-scale angular acceleration on earth, radians per second <sup>2</sup>
$\dot{q}_p$	full-scale angular acceleration on planet, radians per second <sup>2</sup>
$R$	Reynolds number, $\frac{V_m r_{b,m}}{\text{Kinematic viscosity}}$
$r$	radius perpendicular to axis of symmetry of model, centimeters
$r_{b,m}$	maximum body radius of model, centimeters
$r_{b,p}$	maximum body radius of full-scale configuration, centimeters
$t$	time, seconds
$V_m$	model-scale rate of descent on Earth, centimeters per second
$\dot{V}_m$	time rate of change of model-scale rate of descent, $\frac{dV_m}{dt}$ , centimeters per second <sup>2</sup>
$V_p$	full-scale rate of descent on planet, centimeters per second
$X, Y$	horizontal body axes
$Z$	longitudinal body axis

$z$	distance of center of gravity below plane of maximum diameter, centimeters
$\alpha$	angle of attack of symmetrical axis of model, degrees
$\dot{\alpha}$	time rate of change of angle of attack, radians per second
$\mu_m$	relative density of model on Earth, $\frac{m_m}{\rho_e A_m r_{b,m}}$
$\mu_p$	relative density of full-scale configuration on planet, $\frac{m_p}{\rho_p A_p r_{b,p}}$
$\rho_e$	atmospheric density at sea level on Earth, grams per centimeter <sup>3</sup>
$\rho_p$	atmospheric density at sea level of planet, grams per centimeter <sup>3</sup>

$$C_{m\alpha} = \frac{\partial C_m}{\partial \alpha}$$

$$C_{m\dot{\alpha}} = \frac{\partial C_m}{\partial \left( \frac{\dot{\alpha} r_{b,m}}{2V_m} \right)}$$

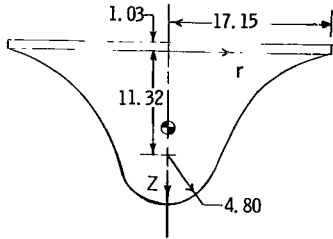
$$C_{mq} = \frac{\partial C_m}{\partial \left( \frac{q r_{b,m}}{2V_m} \right)}$$

## APPARATUS AND TESTS

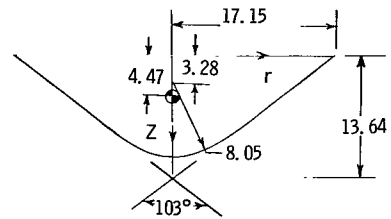
### Models

The models tested were shapes selected to represent a wide variety of possible entry configurations being considered for probes of planetary atmospheres. Drawings of the models are shown in figures 1 and 2. A smaller scale model (5.72 cm radius) of tension shell 0.15 - A 1.05 was also tested. Based on an estimated full-scale diameter of 243.8 cm (8 ft) and model diameters of 34.29 cm to 11.43 cm, the model scales range from 0.141 to 0.047. The ordinates of the tension shell configurations are given in table I and the mass and inertia characteristics of the various models used in this investigation are presented in table II. Two of the tension shell models were tested for a range of center-of-gravity positions; consequently, the center-of-gravity location is not given for these configurations in figure 1. Data for the other models are presented only for the center-of-gravity position shown in figure 1.

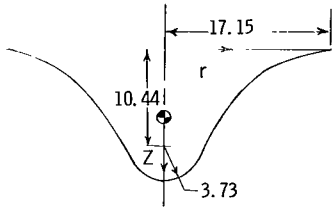
Tension shell 0 - A 1.50



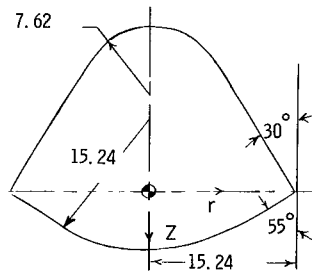
103° cone



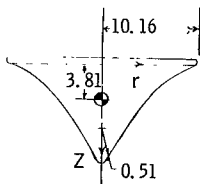
Tension shell .15 - A 1.05



110° cone with afterbody



Tension shell 0 - A 1.40



Apollo-type

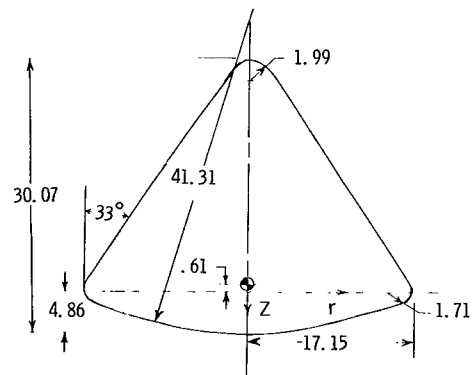
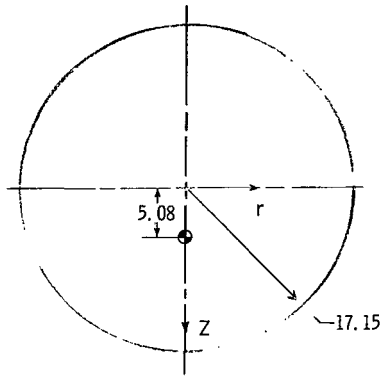
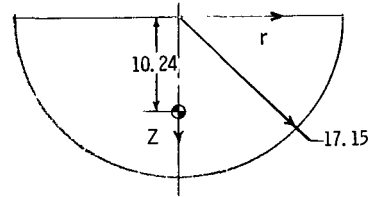


Figure 1.- Models of configurations tested. All dimensions are in centimeters model scale. All models shown are symmetrical about the Z axis.

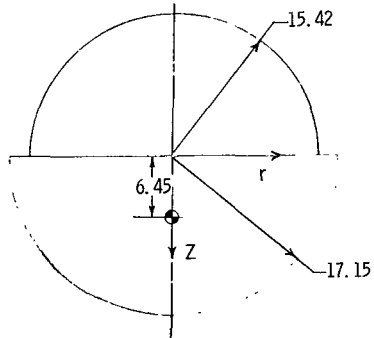
Sphere



Hemisphere



Step-sphere



Torus-sphere

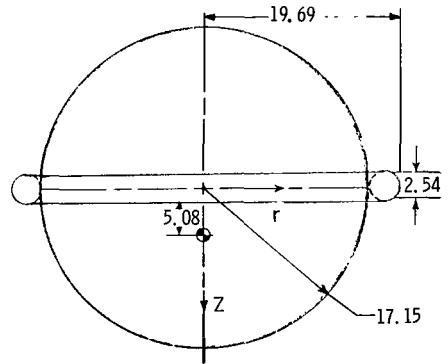


Figure 1.- Concluded.

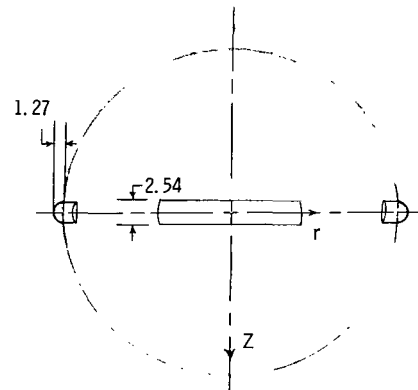
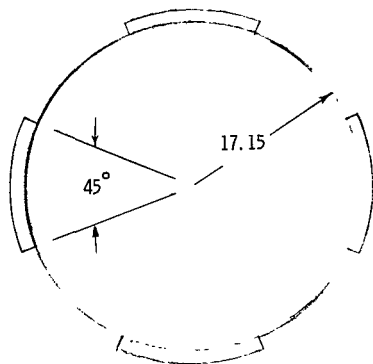


Figure 2.- Two-view drawing of the model of a sphere modified by four  $45^\circ$  partial segments of a torus. All dimensions are in centimeters model scale.



TABLE I.- COORDINATES OF TENSION SHELL MODELS

r/r <sub>b,m</sub>	z/r <sub>b,m</sub> for -		
	Tension shell 0 - A 1.50	Tension shell 0.15 - A 1.05	Tension shell 0 - A 1.40
0	1.284	-----	1.1597
.05	1.177	-----	1.0646
.10	1.071	-----	.9702
.15	.968	0.8332	.8774
.20	.866	.6960	.7866
.25	.768	.5931	.6989
.30	.675	.5069	.6148
.35	.585	.4315	.5343
.40	.501	.3646	.4586
.45	.423	.3047	.3878
.50	.351	.2510	.3223
.55	.285	.2030	.2625
.60	.226	.1604	.2085
.65	.174	.1229	.1605
.70	.128	.0906	.1185
.75	.089	.0631	.0829
.80	.058	.0406	.0534
.85	.033	.0230	.0303
.90	.015	.0103	.0136
.95	.004	.0026	.0034
1.00	0	0	0

Tests

The investigation was conducted in the Langley spin tunnel, which is an atmospheric wind tunnel with a vertically rising airstream and a maximum airspeed of approximately 30 m/sec. The various models were tested in free vertical descent to determine qualitatively the dynamic stability characteristics of the various configurations in vertical descent. The general test procedure used in the vertical tunnel is described in reference 2. For this investigation, the model was hand launched into the vertically rising airstream. Immediately before a model is launched, the model launcher places the model into the tunnel and the tunnel operator increases the velocity of the tunnel airstream until the weight of the model appears to be supported by the dynamic pressure on the model. Immediately after the model is launched, the tunnel operator makes whatever corrections are necessary in the velocity of the tunnel airstream in order to support the model at eye level in the tunnel. The motions of the model are recorded by a motion-picture camera and the film records are used to obtain data such as the frequency and maximum amplitude of oscillations of the models. At times the model was launched erect with as little disturbance as possible to determine whether motions of the capsule were self-excited. At other times the model was launched in an inverted attitude to determine whether it would turn over and stabilize in an erect attitude.

TABLE II. - MASS AND INERTIA CHARACTERISTICS FOR LOADINGS TESTED

[Values given are model scale and moments of inertia are about the center of gravity]

Configuration	Model radius, $r_{b,m}$ , cm	Loading	Actual mass, g	Simulated mass, g	Vertical location of center of gravity measured from plane of maximum diameter, $z/r_{b,m}$	Simulated atmospheric pressure, millibars	Moments of inertia, g-cm <sup>2</sup>		
							$I_X$	$I_Y$	$I_Z$
Tension shell 0 - A 1.50	17.15	1	1035	2797	0.573	144	75 077	75 077	67 632
		2	1547	4181	.521	97	110 903	110 903	94 142
		3	3470	3470	.497	116	116 174	116 174	123 290
		4	1247	3370	.478	120	106 942	106 942	93 690
		5	1547	4181	.435	97	110 903	110 903	94 142
Tension shell 0.15 - A 1.05	17.15	1	2675	7230	0.456	56	91 884	91 884	101 522
		2	2499	6754	.361	60	112 284	112 284	161 496
	5.72	3	97	262	0.502	57	308	308	326
		4	338	913	.276	16.8	770	770	815
Tension shell 0 - A 1.40	10.16	1	783	2116	0.376	40	17 099	17 099	20 034
103° cone	17.15	1	1767	4776	0.260	85	129 122	129 122	204 032
110° cone with afterbody	15.24	1	1072	2897	0.106	98	86 168	86 168	98 606
		2	763	2062	0	138	79 295	79 295	98 606
		3	819	2214	-.085	128	97 741	97 741	98 606
Apollo-type	17.15	1	1533	4143	-0.036	97	225 696	225 696	224 593
Sphere	17.15	1	1225	3311	0.296	122	255 535	255 535	168 587
Step-sphere	17.15	1	1654	4470	0.376	90	255 987	255 987	190 096
Hemisphere	17.15	1	1303	3522	0.597	115	121 103	121 103	143 451
Torus-sphere	19.69	1	1624	4389	0.187	92	282 064	282 064	202 129
Modified torus-sphere	17.15	1	1564	4227	0.216	96	265 354	265 354	179 032

Of particular interest during this study were the drag coefficients of the capsules, the maximum amplitude of the oscillations of the capsules due to self-excited motions, and the ability of the capsules to return to a stable mode of descent after being forced into a tumbling motion by a sudden external force or by launching in an inverted attitude.

These studies were of an exploratory nature and effort was concentrated on the more promising configurations, whereas the less promising were tested only briefly. The desired characteristics were stability and high drag coefficient during vertical descent. During the study, tests were conducted at various simulated atmospheric pressures ranging from 16.8 millibars to 144 millibars, based on a full-scale Earth weight of 1423 N (320 lb). This range of pressure was considered, at the time of the tests, to include the likely range of Martian atmospheric pressures. More recent estimates of the Martian atmospheric pressure place it below this range, however (5 to 10 millibars). The 0.047-scale model of tension shell 0.15 - A 1.05 was constructed specifically to obtain data at simulated atmospheric pressures of less than 40 millibars. This model

also was ballasted to be dynamically similar to the 0.141-scale model of tension shell 0.15 - A 1.05 in order to investigate the possibility of scale effects between the models of different scale. The Reynolds number range of the tests was in the region of 45 000 to 328 000, based on the maximum body radii of the models.

### Accuracy

The characteristics of the models shown in table II are measured to an accuracy of  $\pm 1$  percent for the mass,  $\pm 1$  percent for  $z$ ,  $\pm 10$  percent for the moments of inertia of the 0.047-scale model, and  $\pm 5$  percent for the moments of inertia of all other models. The results presented are estimated to be accurate within  $\pm 1^\circ$  for the maximum amplitude of oscillation,  $\pm 2$  percent for the oscillation frequency, and  $\pm 5$  percent for the drag coefficient.

### Scaling

During the present tests, the density of the models was generally maintained as high as possible within the limits of the spin tunnel. Increasing the density of dynamic models to obtain the desired ratio of model density to atmospheric density has been the method used to simulate high altitudes in the Earth atmosphere, as is indicated in reference 2, and the same principle was used to simulate a planetary atmosphere thinner than that of the Earth during the present tests. During the investigation, it was also necessary to consider the effect of the gravitational fields on planets other than the Earth. It is shown in the appendix that, in general, it is not necessary for this type of tests, to make any changes in models being tested to correct for the different gravitational fields. The correction for the different gravitational fields can be applied as the test data are being converted from model-scale to full-scale values.

The simulation of motions of flight vehicles in thin atmospheres in the spin tunnel is limited to equilibrium rates of descent which are below the maximum velocity of the vertically rising airstream which is about 30 m/sec. Thus, the model rate of descent, in the Earth gravitational field, of a configuration designed to have a full-scale equilibrium rate of descent in the environment of another planet on the order of a hundred meters per second might be so high that only an extremely small-scale model could be tested in the spin tunnel. The practicality of dynamic model tests is in turn limited to models of a reasonable size, so that it is possible to construct a model with proper mass characteristics and sufficient strength to withstand the hazards of testing.

For the present tests the rate of descent of a 0.047-scale dynamic model ballasted to simulate an assumed atmospheric pressure of 17 millibars would be approximately 40 m/sec. As explained in the appendix, extending the effective range of the spin tunnel for tests of this nature is possible by reducing the mass of the dynamic model by the

ratio of the gravitational field on the planet of interest to that on Earth while maintaining the normal dynamically scaled moments of inertia. This procedure results in a model which simulates the equilibrium rate of descent and the rotational motions of a dynamic model on a particular planet. Any linear accelerations of the model during tunnel tests, however, are increased by the ratio of the true dynamic scale mass of the model to the reduced mass used for such tests. As an example of the use of the reduced-weight method in the present tests, the mass of the models was generally reduced to 0.37 that of a true dynamic model and the rate of descent of the most dense 0.047-scale model was, in this way, reduced from approximately 40 m/sec (beyond tunnel capacity) to approximately 25 m/sec. As the moments of inertia were held near their true scale value and as the models did not undergo any noticeable linear accelerations during the tests, the results of these tests should be representative of the performance of a dynamic model on Mars in the assumed atmospheric pressure environment.

### RESULTS AND DISCUSSION

The motions of the models while in simulated vertical descent generally consisted of limit-cycle oscillations with maximum amplitudes of  $\pm 10^\circ$  to  $\pm 20^\circ$ . Sample time histories of these oscillations are shown in figure 3. Only the angular motions are plotted since the sidewise motions of the model were virtually nil. The amplitude of the oscillations was not constant, perhaps because of disturbances caused by the turbulent separated flow behind the model. Actually the amplitude of the oscillations sometimes varied by a factor of about 2 for a given condition.

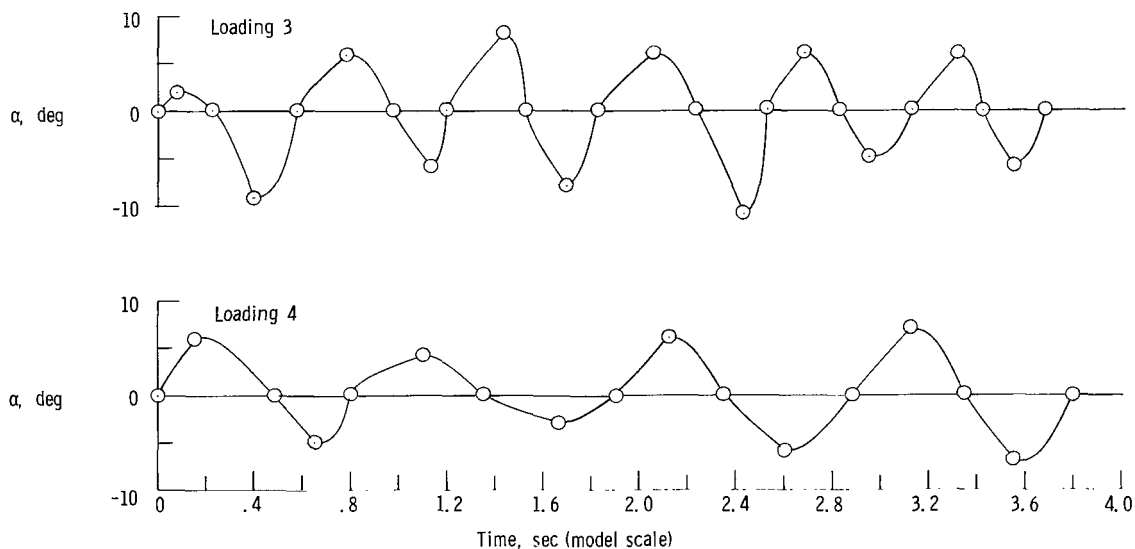


Figure 3.- Sample time histories. Tension shell 0 - A 1.50. Comparison of oscillation frequency for different scaling systems used.

TABLE III.- STABILITY CHARACTERISTICS AND DRAG COEFFICIENT

Configuration	Loading	Maximum amplitude of oscillations, deg	Oscillation frequency, cps, for -		Recovery from inverted launch	V <sub>m</sub> , m/sec	C <sub>D</sub>	R
			Actual model scale	Scaled up to be representative of 0.141-scale model				
Tension shell 0 - A 1.50	1	<20	1.17	1.17	No	13.6	0.97	160 000
	2	<15	1.10	1.10	No	16.7		196 000
	3	<15	1.65	1.65	No	25.0		293 000
	4	<15	1.05	1.05	No	14.9		175 000
	5	<20	.93	.93	No	16.7		196 000
Tension shell 0.15 - A 1.05	1	<15	1.40	1.40	No	20.7	1.15	243 000
	2	<20	1.10	1.10	No	19.8		232 000
	3	<10	2.69	1.55	No	11.6		45 000
	4	<15	2.53	1.46	No	20.4		80 000
Tension shell 0 - A 1.40	1	<15	1.40	1.08	No	20.8	0.89	145 000
103° cone	1	<15	1.43	1.43	No	19.8	0.78	232 000
110° cone with afterbody	1	<15	1.14	1.07	No	15.6	0.97	163 000
	2	-----	.99	.93	---	13.2		138 000
	3	Tumbles	.91	.86	---	13.6		142 000
Apollo-type	1	Tumbles	0.99	0.99	---	17.1	0.93	201 000
Sphere	1	-----	---	---	Yes	28.0	0.27	328 000
Step-sphere	1	<10	1.97	1.97	Yes	23.8	0.50	279 000
Hemisphere	1	<10	---	---	No	22.9	0.43	269 000
Torus-sphere	1	<15	1.05	1.05	Yes	17.0	0.74	214 000
Modified torus-sphere	1	-----	---	---	Yes	23.2	0.50	272 000

Table III presents a summary of the results for the eleven configurations. It indicates the maximum amplitude of the oscillations, the ability of the models to return to a stable erect attitude after an inverted launch, and the drag coefficient in free descent - including the effects of the motions of the model on drag.

#### Tension Shells and 103° Cone

The results of the tests for the three tension shell configurations and the somewhat similar 103° blunted cone showed that these configurations were stable when launched in an erect, or nearly erect, position because large-amplitude initial motions quickly damped down to a limit-cycle oscillation with an amplitude of less than  $\pm 20^\circ$ , as is indicated in table III. These configurations will not return to an erect position, however, if launched in an inverted attitude but will begin to tumble after several cycles of increasingly large amplitude oscillations. The results of table III also indicate that the stability of these configurations was not changed appreciably by varying the location of the center of gravity over the range tested. (Note that the center-of-gravity location was varied

only for tension shell configurations 0 - A 1.50 and 0.15 - A 1.05.) The weight of the models varied somewhat as the center-of-gravity location was varied, but this variation in weight would not be expected to affect the amplitude of the motions as is explained in the appendix in the discussion of the reduced-weight method of scaling.

As mentioned previously, a 0.141-scale and a 0.047-scale model of tension shell 0.15 - A 1.05 were tested, the smaller model being designed to allow the simulation of a less dense atmosphere. The results of these tests are presented in table III which shows the oscillation frequency both in actual model scale and with the frequencies of the 0.047-scale model scaled to be representative of a 0.141-scale model. When the two models were dynamically similar (loadings 1 and 3), the results indicate no significant scale effects between the models. When the 0.141-scale model was tested at a simulated atmospheric pressure of 60 millibars and the 0.047-scale model was tested at a simulated atmospheric pressure of 16.8 millibars (loadings 2 and 4), the results indicated no significant effects due to changes in the simulated atmospheric pressure.

There were significant differences in the drag coefficient of the tension shell and the 103° cone configurations, as shown in table III, with the highest drag coefficient (tension shell 0.15 - A 1.05) being nearly 50 percent greater than the lowest drag coefficient (103° cone).

#### 110° Cone With Afterbody and Apollo-Type Configurations

The results obtained with the superficially similar 110° blunted cone with a conical afterbody and the Apollo-type configurations appear to be similar. The drag values, as shown in table III, were very nearly the same. Also both configurations had similar instabilities with the center of gravity above the maximum diameter station. The motions for this condition were self-excited and the models would begin to tumble after several increasingly large amplitude oscillations when launched in a steady erect attitude. For the 110° cone the oscillations were marginally stable when the center of gravity was located at the maximum diameter station, and they were stable with an amplitude of less than  $\pm 15^\circ$  when the center of gravity was located  $0.106r_{b,m}$  forward of the maximum diameter station. No such forward positions of the center of gravity were tested for the Apollo-type configuration because they appeared to be unreasonably close to the forward end of the vehicle on the basis of its geometry.

#### Sphere, Step-Sphere, Hemisphere

The results of the study of the sphere, the step-sphere, and the hemisphere indicate that the hemisphere which forms the nose of these three configurations does not produce a high drag coefficient. The drag coefficient of the sphere was less than one-third that of the tension shells. The drag coefficients of the step-sphere and the hemisphere, although

low, were significantly greater than that of the sphere, apparently due to the difference in the location of the point of separation of flow on these models and on the sphere.

The sphere exhibited erratic translational motions during vertical descent, even with the center-of-gravity location of the sphere  $0.296r_{b,m}$  below the maximum diameter station, evidently because of erratic shifts in the point of separation of flow from the rearward part of the sphere. This characteristic has been observed by a number of investigators in the past and has, at times, been avoided by such devices as dimpling the surface as in the case of golf balls. No oscillation angles were measured because of the erratic nature of the motions of this model. The oscillations of the step-sphere and the hemisphere were different from those of the sphere in that they did not have the large sidewise motions which were characteristic of the sphere. Both configurations, however, would oscillate at times, and at other times, would rotate such that the axis of symmetry of the model would describe a conical shape. The amplitude of the oscillation was generally less than  $\pm 10^\circ$ , and the half-angle of the conical shape described by the axis of symmetry was generally less than  $10^\circ$  for both configurations.

#### Modified Spheres

The results of the study of a sphere modified by a torus tangent to the equator of the sphere to fix the flow separation point indicated that this configuration was quite stable. The amplitude of oscillations was generally less than  $\pm 20^\circ$  and the model would return to an erect attitude if launched inverted. The drag coefficient, based on the overall diameter of the configuration, was approximately 0.74, which is about two-thirds that of the tension-shell configuration with the highest drag.

The results of the study of a sphere modified by four  $45^\circ$  partial segments of a torus (fig. 2) indicate that this configuration is similar in stability characteristics to a sphere. This modified sphere exhibited erratic translational motions during vertical descent even with the center-of-gravity location of the modified sphere  $0.216r_{b,m}$  below the maximum diameter station. The drag coefficient of this modified sphere was approximately 0.5.

#### CONCLUSIONS

The following conclusions are drawn from the results of a subsonic dynamic model study conducted in the Langley spin tunnel on a number of models of planetary entry capsule configurations:

1. The tension shell and  $103^\circ$  cone configurations have a limit-cycle oscillation of less than  $\pm 20^\circ$ , when launched in a nearly erect attitude, but they are unstable and will tumble if launched in an inverted attitude. The tension shells have the highest drag

coefficients of all the stable configurations tested. Moderate variations of center-of-gravity location, and variations of simulated atmospheric pressure from 17 to 57 millibars did not appreciably affect the stability of the tension shell configurations for which these variations were tested.

2. The  $110^\circ$  blunted cone with a conical afterbody is stable if launched erect with the center of gravity forward of the maximum diameter station but it will tumble if launched inverted. With the center of gravity above the maximum diameter station, however, this configuration is unstable and tumbles – as is also the case for the somewhat similar Apollo-type configuration.

3. In general the various configurations derived from a sphere have markedly lower drag than the other configurations and no better stability. The sphere with a torus around its equator was the best of these configurations; it would return to an erect attitude if launched inverted, but its drag was only about two-thirds that of the highest-drag tension shell.

4. The reduced-weight scaling method offers the advantage of lower equilibrium rates of descent during model tests. This method, however, will cause any linear accelerations of the model to be increased by the ratio of the true dynamic scale mass of the model to the reduced mass used for such tests.

Langley Research Center,  
National Aeronautics and Space Administration,  
Langley Station, Hampton, Va., February 25, 1966.



## APPENDIX

### MODEL SCALING TECHNIQUES FOR STUDIES OF MOTIONS OF VEHICLES IN VERTICAL DESCENT IN PLANETARY ENVIRONMENTS OTHER THAN THAT OF THE EARTH

Previous investigations in the Langley spin tunnel have repeatedly demonstrated the feasibility of simulating motions of aircraft and spacecraft in the Earth's environment by means of small-scale dynamic model tests. (See, for example, refs. 2, 3, and 4.) Predicting motions of vehicles in other planetary environments from the results of dynamic model tests conducted on Earth is complicated by the inability to alter the Earth's gravitational field. In this appendix, an analysis is made to determine (1) methods of analyzing Earth dynamic model test results to predict motions of vehicles descending at equilibrium rates of descent in other planetary environments and (2) what, if any, changes from conventional dynamic-model-ballasting and test-result-scaling techniques are desirable and practical with regard to better obtaining the desired information.

Equations of motion which are applicable to the present model tests can be found in reference 2. These are the force equations which describe equilibrium rate of descent and a moment equation which describes motion about an arbitrary horizontal axis. As applied to the present investigation, these equations are:

$$\dot{V}_m = -\frac{\rho_e V_m^2 A_m}{2m_m} C_D + g_e \quad (1)$$

$$\dot{q}_m = \frac{\rho_e V_m^2 A_m r_{b,m}}{2m_m k_m^2} C_m \quad (2)$$

As this discussion must be restricted to equilibrium rate of descent,  $\dot{V}_m$  would vanish and equation (1) reduces to

$$m_m g_e = \frac{\rho_e V_m^2 A_m}{2} C_D$$

or

$$V_m = \left( \frac{2m_m g_e}{\rho_e A_m C_D} \right)^{1/2} \quad (3)$$

## APPENDIX

Substituting equation (3) into equation (2) eliminates the velocity term from equation (2) and yields

$$\dot{q}_m = \frac{r_{b,m} g_e}{k_m} \frac{C_m}{C_D} \quad (4)$$

A third equation which describes the motion observed during the present tests is the classical stability theory equation for the frequency of an oscillatory motion sustained by linearized aerodynamic inputs,

$$f_m = \left[ \left( \frac{C_{m_q} + C_{m_{\dot{\alpha}}}}{8\mu_m k_m / r_{b,m}} \right)^2 + \frac{C_{m_\alpha}}{2\mu_m k_m / r_{b,m}} \right]^{1/2} \frac{V_m}{r_{b,m}}$$

Substituting equation (3) into this equation eliminates the velocity term and yields

$$f_m = \left[ \left( \frac{C_{m_q} + C_{m_{\dot{\alpha}}}}{8\mu_m k_m / r_{b,m}} \right)^2 + \frac{C_{m_\alpha}}{2\mu_m k_m / r_{b,m}} \right]^{1/2} \frac{1}{r_{b,m}} \left( \frac{2m_m g_e}{\rho_e A_m C_D} \right)^{1/2} \quad (5)$$

Equations (3) to (5) indicate that, for dynamic model tests in which equilibrium exists between the weight of the model and the aerodynamic force due to the dynamic pressure on the model, the simulated equilibrium rate of descent, the angular accelerations, and the oscillation frequency of the model are all dependent on the magnitude of the gravitational field in which the tests are conducted. The manner in which these dependencies affect data scaling methods when conventional Earth dynamic models are used to obtain data applicable to the environment of another planet, may be seen in the section which follows.

### Earth Dynamic-Model Method

The conventional Earth dynamic-model method is discussed at length in reference 5. It will suffice here to say that the mass and inertia characteristics of a dynamic model are determined according to the following equations:

$$m_m = m_p N^3 \frac{\rho_e}{\rho_p} \quad (6)$$

APPENDIX

$$I_m = I_p N^5 \frac{\rho_e}{\rho_p} \quad (7)$$

From these equations and the geometric relations between the full-scale configuration and the model, the following additional relationships are obtained:

$$r_{b,m} = N r_{b,p} \quad (8)$$

$$A_m = N^2 A_p \quad (9)$$

$$\mu_m = \mu_p \quad (10)$$

$$k_m = N k_p \quad (11)$$

Equations (6) to (11) can be utilized to reduce equations (3), (4), and (5) to

$$V_m = \left( \frac{2m_p g_p}{\rho_p A_p C_D} \right)^{1/2} N^{1/2} \left( \frac{g_e}{g_p} \right)^{1/2}$$

$$\dot{q}_m = \frac{r_{b,p} g_p}{k_p^2} N^{-1} \frac{g_e}{g_p} \frac{C_m}{C_D}$$

and

$$f_m = \left[ \left( \frac{C_{mq} + C_m \dot{\alpha}}{8\mu_p k_p^2 / r_{b,p}^2} \right)^2 + \frac{C_m \alpha}{2\mu_p k_p^2 / r_{b,p}^2} \right]^{1/2} \frac{1}{r_{b,p}} \left( \frac{2m_p g_p}{\rho_p A_p C_D} \right)^{1/2} N^{-1/2} \left( \frac{g_e}{g_p} \right)^{1/2}$$

Because the collection of terms which make up parts of the right-hand sides of these three equations are the full-scale quantities  $V_p$ ,  $q_p$ , and  $f_p$ , respectively, these equations may be rewritten as

$$V_m = V_p N^{1/2} \left( \frac{g_e}{g_p} \right)^{1/2} \quad (12)$$

$$\dot{q}_m = \dot{q}_p N^{-1} \frac{g_e}{g_p} \quad (13)$$

## APPENDIX

$$f_m = f_p N^{-1/2} \left( \frac{g_e}{g_p} \right)^{1/2} \quad (14)$$

These equations would be used to convert Earth dynamic-model data to full-scale data applicable to the environment of another planet. Unfortunately, limitations in the equilibrium rate of vertical descent which can be simulated in the spin tunnel tend to make this technique impractical. The desired high equilibrium rates of descent result from the necessity of simulating planetary atmosphere much thinner than that of the Earth. The method used to simulate less dense atmosphere (which are associated with high altitudes in the Earth's atmosphere in the discussion of ref. 2) is to increase the density of a dynamic model to obtain the desired ratio of model density to atmospheric density. This increase is associated with the term  $\rho_e/\rho_p$  in equations (6) and (7). A thin planetary atmosphere frequently results in part from a weak gravitational field and this weak gravitational field does allow compensation in terms of reduced weight in the design of a test model as may be seen in the section which follows.

### Reduced-Weight Method

A reduced-weight method of model preparation was derived which resulted in a reduction in the equilibrium rate of descent of the model during spin tunnel tests, such that the combination of a lower atmospheric density and a field could be simulated. The mass and inertia characteristics of the model (which shall be referred to as a pseudo-dynamic model) are determined according to the following equations:

$$m_m = m_p N^3 \frac{\rho_e}{\rho_p} \frac{g_p}{g_e} \quad (15)$$

$$I_m = I_p N^5 \frac{\rho_e}{\rho_p} \quad (7)$$

From these equations and the geometric relations between the full-scale configuration and the model, the following additional relationships are obtained:

$$r_{b,m} = N r_{b,p} \quad (8)$$

$$A_m = N^2 A_p \quad (9)$$

$$\mu_m = \mu_p \frac{g_p}{g_e} \quad (16)$$

## APPENDIX

$$k_m = Nk_p \left( \frac{g_e}{g_p} \right)^{1/2} \quad (17)$$

Equations (8) and (9) and equations (15), (16), and (17) can be utilized to reduce equations (3), (4), and (5) to the following form:

$$V_m = \left( \frac{2m_p g_p}{\rho_p A_p C_D} \right)^{1/2} N^{1/2}$$

$$\dot{q}_m = \frac{r_{b,p} g_p}{k_p^2} N^{-1} \frac{C_m}{C_D}$$

$$f_m = \left[ \left( \frac{C_{m_q} + C_{m \dot{q}}}{8\mu_p k_p^2 / r_{b,p}^2} \right)^2 + \frac{C_{m \alpha}}{2\mu_p k_p^2 / r_{b,p}^2} \right]^{1/2} \frac{1}{r_{b,p}} \left( \frac{2m_p g_p}{\rho_p A_p C_D} \right)^{1/2} N^{-1/2}$$

By collecting terms as was done to obtain equations (12), (13), and (14), these equations can be rewritten as:

$$V_m = V_p N^{1/2} \quad (18)$$

$$\dot{q}_m = \dot{q}_p N^{-1} \quad (19)$$

$$f_m = f_p N^{-1/2} \quad (20)$$

A comparison of these three equations with equations (12), (13), and (14) shows that the various terms involving  $g_e/g_p$  have been eliminated. Thus, the rate of descent, the angular accelerations, and the frequency of oscillation of the pseudodynamic model on Earth will be identical to the corresponding quantities that would be obtained were it possible to test a dynamic model on another planet. In addition, the oscillation amplitudes of the pseudodynamic model on Earth should also be identical to that of a dynamic model on the other planet.

### Comparison of Scaling Methods

Brief tests were conducted with tension shell 0 - A 1.50 loaded by both the Earth dynamic-model and the reduced-weight method in order to obtain data for a comparison of the results. The model motions are indicated in the time histories of figure 3.


## APPENDIX

Loading 3, indicated in figure 3, represents results obtained by using the Earth dynamic-model method; and loading 4 represents results obtained by using the reduced-weight method. Specifically, loading 4 was similar to loading 3 with respect to center-of-gravity location and moments of inertia, but the weight was reduced to approximately  $g_p/g_e$  or 0.37 that of loading 3. The data of figure 3 show that the maximum amplitude of the model oscillations was not affected by the difference in model weighting technique, but that the frequency of the oscillations was markedly affected. Upon examination of these results and by applying equations (14) and (20), it was found that this difference in frequency was of the magnitude that would be expected from the difference in model weighting techniques. The ratio of the oscillation frequencies shown in figure 3 would be expected to be approximately  $\sqrt{0.37}$  or 0.61 and was in fact 0.64.

In general, the use of the reduced-weight method for model tests during which there were significant linear accelerations of the model would result in these accelerations being scaled up inversely to the reduction in mass of the model. For this reason, the exact method of simulation would be preferred unless the atmospheric density to be simulated is so low that the reduced-weight method is necessary.

## REFERENCES

1. Roberts, Leonard: Entry Into Planetary Atmospheres. *Astronaut. Aeron.*, vol. 2, no. 10, Oct. 1964, pp. 22-29.
2. Neihouse, Anshal I.; Klinar, Walter J.; and Scher, Stanley H.: Status of Spin Research for Recent Airplane Designs. NASA TR R-57, 1960. (Supersedes NACA RM L57F12.)
3. Bowman, James S., Jr.: Dynamic Model Tests at Low Subsonic Speeds of Project Mercury Capsule Configurations With and Without Drogue Parachutes. NASA TM X-459, 1961.
4. Lee, Henry A.; Costigan, Peter J.; and Bowman, James S., Jr.: Dynamic-Model Investigation of a 1/20-Scale Gemini Spacecraft in the Langley Spin Tunnel. NASA TN D-2191, 1964.
5. Scherberg, Max; and Rhode, R. V.: Mass Distribution and Performance of Free Flight Models. NACA TN 268, 1927.



*"The aeronautical and space activities of the United States shall be conducted so as to contribute . . . to the expansion of human knowledge of phenomena in the atmosphere and space. The Administration shall provide for the widest practicable and appropriate dissemination of information concerning its activities and the results thereof."*

—NATIONAL AERONAUTICS AND SPACE ACT OF 1958

## NASA SCIENTIFIC AND TECHNICAL PUBLICATIONS

**TECHNICAL REPORTS:** Scientific and technical information considered important, complete, and a lasting contribution to existing knowledge.

**TECHNICAL NOTES:** Information less broad in scope but nevertheless of importance as a contribution to existing knowledge.

**TECHNICAL MEMORANDUMS:** Information receiving limited distribution because of preliminary data, security classification, or other reasons.

**CONTRACTOR REPORTS:** Technical information generated in connection with a NASA contract or grant and released under NASA auspices.

**TECHNICAL TRANSLATIONS:** Information published in a foreign language considered to merit NASA distribution in English.

**TECHNICAL REPRINTS:** Information derived from NASA activities and initially published in the form of journal articles.

**SPECIAL PUBLICATIONS:** Information derived from or of value to NASA activities but not necessarily reporting the results of individual NASA-programmed scientific efforts. Publications include conference proceedings, monographs, data compilations, handbooks, sourcebooks, and special bibliographies.

*Details on the availability of these publications may be obtained from:*

SCIENTIFIC AND TECHNICAL INFORMATION DIVISION  
NATIONAL AERONAUTICS AND SPACE ADMINISTRATION  
Washington, D.C. 20546